Stetler, D. A., & Rose, K. M. (1983) *Biochim. Biophys. Acta 739*, 105-113.
Tabor, C. W., & Tabor, H. (1984) *Annu. Rev. Biochem. 53*, 749-790.
Takio, K., Kuenzel, E. A., Walsh, K. A., & Krebs, E. G. (1987) *Proc. Natl. Acad. Sci. U.S.A. 84*, 4851-4855.
Walton, G. M., & Gill, G. N. (1983) *J. Biol. Chem. 258*, 4440-4446.
Zandomeni, R., Zandomeni, M. C., Shugar, D., & Weinmann, R. (1986) *J. Biol. Chem. 261*, 3414-3419.
Zalta, J., Zalta, J. P., & Simard, R. (1971) *J. Cell Biol. 51*, 563-568.

Spectroscopic and Kinetic Characterization of Nonenzymic and Aldose Reductase Mediated Covalent NADP-Glycolaldehyde Adduct Formation†

C. E. Grimshaw,* M. Shahbaz,‡ and C. G. Putney
Department of Molecular and Experimental Medicine, Division of Biochemistry, Research Institute of Scripps Clinic, Scripps Clinic and Research Foundation, La Jolla, California 92037

Received August 21, 1989; Revised Manuscript Received July 2, 1990

ABSTRACT: Reaction of glycolaldehyde with the binary E·NADP complex of bovine kidney aldose reductase (ALR2) produces an enzyme-bound chromophore whose absorbance (λ_{max} 341 nm) and fluorescence (λ^{ex}_{max} 341 nm; λ^{emit}_{max} 421 nm) properties are distinct from those of NADPH or E·NADPH yet are consistent with the proposed covalent adduct structure [1,4-dihydro-4-(1-hydroxy-2-oxoethyl)nicotinamide adenine dinucleotide phosphate]. The kinetics of adduct formation, both in solution and at the enzyme active site, support a mechanism involving rate-determining enolization of glycolaldehyde at high [$NADP^+$] or [E·NADP]. At low [$NADP^+$] or [E·NADP] the reaction is second-order overall, but the ALR2-mediated reaction displays saturation by glycolaldehyde due to competition of the aldehyde (plus hydrate) and enol for E·NADP. Measurement of the pre-steady-state burst of E·adduct formation confirms that glycolaldehyde enol is the reactive species and gives a value of 1.3×10^{-6} for K_{enol} = [enol]/([aldehyde] + [hydrate]), similar to that determined by trapping the enol with I_3^-. At the ALR2 active site, the rate of adduct formation is enhanced 79 000-fold and the adduct is stabilized ≥13 000-fold relative to the reaction with $NADP^+$ in solution. A portion of this enhancement is ascribed to specific interaction of $NADP^+$ with the enzyme since the 3-acetylpyridine analogue, (AP)ADP^+, gives values that are 15-200-fold lower. Additional evidence for strong interaction of ALR2 with both $NADP^+$ and NADPH is reported. Yet, because dissociation of adduct is slow, catalysis of the *overall* adduct formation reaction by ALR2 is ≤67-fold.

Aldose reductase (ALR2;[1] alditol-$NADP^+$ 1-oxidoreductase; E.C. 1.1.1.21), an NADPH-dependent aldehyde reductase that has received much attention as a potential therapeutic target for the prevention or amelioration of diabetic complications [reviewed in Kador et al. (1985)], displays substrate inhibition by a variety of aldehyde substrates (McKercher et al., 1985; Grimshaw et al., 1989). For two- and three-carbon aldoses, inhibition of the initial reaction rate is followed by a time-dependent onset of further inhibition, reminiscent of the substrate inhibition of lactate dehydrogenase by pyruvate (Gutfreund et al., 1968; Burgner et al., 1978). In that case, substrate inhibition arises from the combination of a rapidly reversible component, due to formation of the dead-end E·NAD·pyruvate complex, and a time-dependent component attributed to reaction of pyruvate enol with E·NAD^+ to produce a covalent NAD-pyruvate adduct at the enzyme active site (Everse et al., 1971a; Sugrobova et al., 1972; Burgner & Ray, 1974). Detailed studies of the latter reaction, both on and off the enzyme, have advanced our understanding of the mechanistic basis for the catalytic efficiency of lactate dehydrogenase (Burgner & Ray, 1974, 1978, 1984a,b; Burgner et al., 1978).

In this paper we present a detailed spectroscopic and kinetic study of the nonenzymic and ALR2-mediated reactions of glycolaldehyde with $NADP^+$ and with the 3-acetylpyridine analogue, (AP)ADP^+. UV-visible and fluorescence results

† This work was supported by a grant to C.E.G. from the National Institute for Diabetes and Digestive and Kidney Diseases (DK 32218) and by the Olive H. Whittier Fund. Support for the VAX 11/750 in the General Clinical Research Center, Scripps Clinic and Research Foundation, was provided by the Division of Research Resources (Grant RR 00833) from the National Institutes of Health. This is publication number 5985-MEM from the Research Institute of Scripps Clinic, Scripps Clinic and Research Foundation.

* Address correspondence to this author.
‡ Present address: Progenix, Inc., La Jolla, CA 92037.

[1] The nomenclature for aldose reductase (ALR2) was recommended by the First International Workshop on Aldehyde Dehydrogenase and Aldehyde Reductase, held in Bern, Switzerland, on July 12-14, 1982 (Turner & Flynn, 1982). Abbreviations: Na_2EDTA, disodium ethylenediaminetetraacetate; Mops, 3-(*N*-morpholino)propanesulfonic acid; NAD^+, β-nicotinamide adenine dinucleotide; NADH, reduced form of NAD^+; $NADP^+$, β-nicotinamide adenine dinucleotide phosphate; NADPH, reduced form of $NADP^+$; N(Hx)DP^+, β-nicotinamide hypoxanthine dinucleotide phosphate; N(Hx)DPH, reduced form of N(Hx)DP^+; (AP)ADP^+, β-3-acetylpyridine adenine dinucleotide phosphate; (AP)ADPH, reduced form of (AP)ADP^+; (AP)AD^+, β-3-acetylpyridine adenine dinucleotide; NADP-ald or simply "adduct", the covalent adduct [1,4-dihydro-4-(1-hydroxy-2-oxoethyl)nicotinamide adenine dinucleotide phosphate]resulting from reaction of glycolaldehyde with $NADP^+$; E·NADP·ald, the ternary dead-end complex of ALR2 with $NADP^+$ and glycolaldehyde; E·NADP-ald, the *binary* E·adduct complex [similar nomenclature is used for adduct and enzyme complexes containing (AP)ADP^+ and N(Hx)DP^+]. Fluorescence data are given as ${}_{ex}F_{emit}$, with λ_{max} for excitation (λ^{ex}_{max}) and emission (λ^{emit}_{max}) shown as preceding and following subscripts, respectively.

0006-2960/90/0429-9936$02.50/0

are shown to be consistent with a proposed structure for the adduct as 1,4-dihydro-4-(1-hydroxy-2-oxoethyl)nicotinamide (or 3-acetylpyridine) adenine dinucleotide phosphate, and the role of glycolaldehyde enol as the reactive intermediate in both reactions is confirmed. In addition, we describe evidence for a strong interaction of the ALR2 active site with both $NADP^+$ and NADPH and compare the binding affinity of several NADP(H) analogues. The kinetic constants described here for ALR2-mediated adduct formation in the absence of glycolaldehyde turnover are used in the second paper (Grimshaw et al., 1990) to interpret the nonlinear kinetics observed for substrate inhibition by glycolaldehyde in the normal enzymic reaction.

Experimental Procedures

Materials. Glycolaldehyde, $NADP^+$, NADPH, $N(Hx)DP^+$, N(Hx)DPH, $(AP)ADP^+$, and NADH were from Sigma. The best available grades of other chemicals, biochemicals, and enzymes were used. Aldose reductase (ALR2), purified from bovine kidney as described previously (Grimshaw et al., 1989), consisted of only "activated form" as determined by active-site fluorescence titration, aldose reductase inhibitor titration, and initial velocity measurements (Grimshaw et al., 1989). When necessary, the enzyme was exchanged into buffer containing 0.5 mM EDTA and either 20 mM Mops or 20 mM sodium phosphate (pH 7.0) by rapid gel filtration through a column (1.0 × 12 cm) of Trisacryl-GF05 resin. Solutions were prepared with distilled, deionized water that had been treated with Chelex-100 resin to remove trace metal ion contaminants (Bio-Rad Laboratories, 1986). pH was measured with a Radiometer PHM 84 pH meter and GKC-2321C combined electrode.

(AP)ADPH was prepared by reduction of 5 μmol of $(AP)ADP^+$ with 50 units of malic enzyme in a total volume of 1.0 mL containing 6 μmol of L-malate, 10 mM $Mg(OAc)_2$, and 20 mM triethanolamine buffer, pH 7.8. Lactate dehydrogenase (50 units) and NADH (5 μmol) were included to prevent nonenzymic adduct formation between $(AP)ADP^+$ and pyruvate (Griffin & Criddle, 1970). The reaction was complete within 5 min, as monitored by the absorbance increase at 390 nm ($\Delta\epsilon_{390nm} \approx 4200\ M^{-1}\ cm^{-1}$). After removal of protein by centrifugal ultrafiltration (Centricon-10), the reaction mixture was fractionated by FPLC (5 × 5 cm Mono-Q column) using the procedure described by Orr and Blanchard (1984) for purification of NADPH. Purified (AP)ADPH ($A_{260}/A_{363} \leq 1.65$) was obtained after a second chromatographic run through the same column.

Fluorescence Titration. The dissociation constant and extent of quenching of the protein fluorescence ($_{285}F_{338}$) for various binary E·nucleotide complexes were determined by using a Perkin-Elmer 650-40 spectrofluorometer equipped with a thermostated cell compartment, as described previously (Grimshaw et al., 1989). Briefly, titrations were carried out by serial addition of aliquots (2 μL) of a concentrated ligand solution (0.1–2 mM) to a 1.0-cm^2 quartz cuvette containing ALR2 (0.5–2.5 μM) in 1.0 mL of MOPSE buffer (50 mM Mops and 0.1 mM Na_2EDTA, pH 7.0) at 15 °C (slits: 2 nm excitation, 10 nm emission). Standard glycyl–tryptophan solutions were used to correct for inner filter and dilution effects. K_d was determined by using eq 1, where $[L]_t$ and $[E]_t$

$$[L]_t/\Theta = K_d/(1 - \Theta) + [E]_t \quad (1)$$

are the total concentrations of ligand and enzyme, respectively, and Θ is the ratio of the observed to the maximum fluorescence change ($\Theta = \Delta F/\Delta F_{max}$) (Stinson & Holbrook, 1973). Quenching was calculated as $Q_{E\cdot L} = (\Delta F_{max}/F_E)$, where $\Delta F_{max} = (F_E - F_{E\cdot L})$ and F_E and $F_{E\cdot L}$ are the observed fluorescence for E and E·L, respectively.

Absorbance and Fluorescence Spectra. Absorbance spectra were measured by using a Hewlett-Packard 8450A double-beam diode array spectrophotometer equipped with custom-designed water-jacketed cell compartments. Absorbance changes resulting from ALR2-mediated adduct formation were determined by using a 1.0-cm path length quartz self-masking microcuvette containing 7.5 μM ALR2, 20 μM $NADP^+$ or $(AP)ADP^+$, and 50 mM glycolaldehyde in a total volume of 0.3 mL of MOPSE buffer at 15 °C. To start the reaction, glycolaldehyde (30 μL) was added first to the reference cell (containing all reagents except ALR2) and immediately thereafter to the sample cell. The initial spectrum [$spectrum_{t=0}$ = $(sample - reference)_{t=0}$], measured within 5 s of glycolaldehyde addition, was stored and subtracted from each subsequent spectrum, thus generating a time course of difference spectra ($spectrum_t - spectrum_{t=0}$). This procedure simplified identification of the small absorbance changes that occur during adduct formation. The reversibility of the observed absorbance changes was established by using tandem-compartment quartz cells as described previously for lactate dehydrogenase mediated adduct formation (Burgner & Ray, 1974). Nonenzymic adduct formation was monitored in a similar manner, except 1.0-cm path length quartz semimicrocuvettes containing 1.0 mL total volume were used, and nucleotide was added last to start the reaction. Absorbance changes due to reaction of glycolaldehyde with adenine-containing nucleotides (Grimshaw et al., 1990) were minimized by including an equivalent level of adenine (as ADP) in the reference mixture for the nonenzymic reactions. The difference spectrum (E·NADP minus free E) was measured by using tandem-compartment quartz cells (0.9-cm total path length) containing ALR2 (17 μM) and $NADP^+$ (40 μM) (MOPSE buffer at 15 °C) on the same side of the sample cell and on opposite sides of the reference cell, respectively.

Uncorrected fluorescence excitation and emission spectra were determined at 25 °C with the apparatus described above. A linear dependence of F_{obs} on $[L]_t$ or $[E\cdot L]_t$ was maintained in all cases. A 2.5:1 ratio of ALR2:nucleotide was used for determination of λ^{ex}_{max} and λ^{emit}_{max} for E·NADPH and E·(AP)-ADPH; computer stimulation showed that $F_{E\cdot nucleotide}$ accounted for ≥96% of F_{obs} under these conditions. For E·adduct, $Q_{E\cdot adduct}$ was calculated from the Q_{obs} for the equilibrium mixture (e.g., E·NADP, E·NADP·ald, and E·adduct) by correcting for the quenching contribution of E·nucleotide and E·nucleotide·ald and normalizing to $[E\cdot adduct]/[E]_t = 1.0$.

Glycolaldehyde Enolization. Glycolaldehyde enol formation was measured by using the method described by Hall and Knowles (1975). Briefly, reactions were conducted in 1.0-cm path length quartz cuvettes at 15 °C in sodium phosphate buffer (5–100 mM, pH 7.0) containing 50 mM sodium iodide and 20 μM I_3^-; initial rates were calculated from the decrease in absorbance due to consumption of I_3^- ($\epsilon_{351nm} = 26\,500\ M^{-1}\ cm^{-1}$; Awtrey & Connick, 1951). The equilibrium enol concentration was estimated by measuring the reaction with the aid of an SFA-11 rapid-mixing device (Hi-Tech Scientific, U.K.), the rapid initial burst being taken as the enol concentration. Pretreatment of the glycolaldehyde stock solution with a 0.03% molar ratio of I_3^- (i.e., to eliminate reactive contaminants) did not affect the size of the burst observed following reequilibration.

Kinetic Studies. Both absorbance and fluorescence methods were used to monitor the rate of adduct formation. For the enzyme-mediated reaction ($[E]_t \geq 3$ μM), digital absorbance

data averaged over the peak of maximum ΔA (e.g., 341 ± 2 nm for E·NADP–ald) were measured as a function of time with a Hewlett-Packard 8450A double-beam diode array spectrophotometer using the protocol described above. Briefly, buffer (30–210 mM Mops or 25–100 mM sodium phosphate containing 0.1 mM Na_2EDTA, pH 7.0), nucleotide (varied to insure that [nucleotide] $\gg K_{dnucleotide}$), and enzyme were preincubated at 15 °C. Reaction was started by addition of glycolaldehyde (at 15 °C; 10–100 mM final concentration) to the reference cell first (containing all but enzyme) and then the sample cell. Initial rates (dA/dt) were estimated by eye, either directly or by linear extrapolation of plots of dA/dt against t to $t = 0$ (Alberty & Koerber, 1957). To convert the observed rates (ΔA s^{-1}) to units of M s^{-1}, we used as $\epsilon_{E\cdot adduct}$ those values reported for the chemically prepared adducts NAD–glyceraldehyde (ϵ_{340nm} = 6300 M^{-1} cm^{-1}; Burton & Kaplan, 1954; Burton et al., 1957) and (AP)AD–pyruvate (ϵ_{365nm} = 10 000 M^{-1} cm^{-1}; DiSabato, 1968).

For $[E]_t \leq 3$ μM, adduct formation was monitored by measuring the increase in E·adduct fluorescence (energy transfer band: $_{285}F_{421}$ for E·NADP–ald, $_{285}F_{445}$ for E·(AP)-ADP–ald). Assays were conducted in 1.0-cm^2 quartz cuvettes in a final volume of 1.0 mL MOPSE buffer, 15 °C, with a full-scale deflection calibrated to equal a 0.10–0.75 μM change in E·adduct. The pre-steady-state burst of E·NADP·ald formation was similarly monitored by using $_{341}F_{421}$. Glycolaldehyde (at 15 °C) was added last to start the reaction, and initial rates were determined as described above. Alternatively, for $[E]_t$ = 0.10–0.625 μM, the full reaction time course was fitted to eq 2, where t is time, k is the first-order rate constant, and Y and Y_{max} are the values of the observed parameter at $t = 0$ and $t = \infty$, respectively.

$$Y = Y_{max}(1 - e^{-kt}) \quad (2)$$

Nonenzymic adduct formation rates were determined from the absorbance increase at 337 ± 2 nm for NADP–ald or N(Hx)DP–ald and 350 ± 2 nm for (AP)ADP–ald by using the ϵ values noted above. Buffer (50–200 mM Mops containing 0.1 mM, Na_2EDTA, pH 7.0) and glycolaldehyde (50–1000 mM) were incubated at 15 °C, nucleotide was added last to start the reaction, and initial rates were estimated as described above. For determination of the equilibrium constant for (AP)ADP–ald formation (K'^{ne}_{eq}), reactions were conducted in capped cuvettes under an inert argon atmosphere and the end point was estimated from the observed ΔA_{350} after 4 half-lives.

The rate constant for E·adduct decomposition was determined from the first-order decay of fluorescence (energy transfer band) after 100-fold dilution of an aliquot of the E·adduct complex (32 μM ALR2, 50 mM glycolaldehyde, and 100 μM $NADP^+$ or $(AP)ADP^+$, incubated at 15 °C for 45 min to establish equilibrium) into MOPSE buffer at 15 °C (final concentrations: [nucleotide] = 1 μM, [ald] = 0.5 mM, and [ALR2] = 0.32 μM in 50 mM Mops and 0.1 mM Na_2-EDTA, pH 7.0). The reaction time course was fitted to eq 2.

Data Processing. Data were fitted to the equations in the text by the least-squares method using the Fortran programs of Cleland (1979). Buffer catalysis was analyzed by using eq 3, where k_0 is the value of k at [buffer] = 0. Data showing saturation kinetics for A were fitted to eq 4, where V is the maximum value of v_i and K_a is the apparent half-saturation constant for A.

$$k = k_0 + k_B[\text{buffer}] \quad (3)$$

$$v_i = VA/(K_a + A) \quad (4)$$

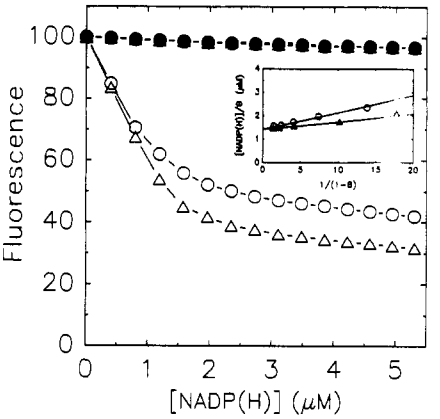

FIGURE 1: $NADP^+$ and NADPH binding to ALR2 determined by fluorescence titration. Quenching of the ALR2 protein fluorescence ($_{285}F_{338}$) due to binding of $NADP^+$ (O) or NADPH (Δ) was monitored following addition of 2-μL aliquots of a 200 μM stock nucleotide solution to 1.0 mL of MOPSE buffer containing 1.4 μM ALR2 at 15 °C. Titration of a standard glycyl–tryptophan solution (filled symbols) was used to correct for inner filter and dilution effects. Inset shows least-squares fits of the corrected data ($\theta = \Delta F/\Delta F_{max}$) to eq 1 (Stinson & Holbrook, 1973) with K_{dNADP} = 0.07 ± 0.02 μM and K_{dNADPH} = 0.03 ± 0.01 μM. Data shown are for a representative titration; Table I lists the K_d values averaged over several ($n \geq 3$) determinations.

Table I: Equilibrium Dissociation Constants for Nucleotides

nucleotide	K_d[a] (μM)
$NADP^+$	0.080 ± 0.030
NADPH	0.046 ± 0.015
$(AP)ADP^+$	0.24 ± 0.03
(AP)ADPH	0.22 ± 0.04
$N(Hx)DP^+$	290 ± 30
N(Hx)DPH	≥300[b]

[a] K_d values determined from fits to eq 1 of data for quenching of protein fluorescence (MOPSE buffer, 15 °C). [b] Lower limit only, due to large inner filter effect.

Results

Equilibrium Dissociation Constants. The quenching of protein fluorescence ($_{285}F_{338}$) upon binding NADPH or $NADP^+$ to ALR2 (Figure 1) was analyzed by using eq 1 (inset, Figure 1). As shown in Table I, K_d measured at 15 °C (MOPSE buffer) was less than 0.1 μM for both $NADP^+$ and NADPH. Comparison of the K_d values for the alternate nucleotides further shows that the ALR2 binding site will readily tolerate changes in the nicotinamide side chain [e.g., (AP)ADPH versus NADPH] but not in the adenine moiety [e.g., N(Hx)DPH versus NADPH]. Quenching of the protein fluorescence observed for oxidized nucleotides (e.g., $NADP^+$; see Figure 1) can be ascribed to the formation of a broad absorption band centered at 366 nm ($\epsilon \approx 1400$ M^{-1} cm^{-1}) in the binary E·NADP complex (Figure 2).

Absorbance Spectra. Reaction of glycolaldehyde with E·NADP or E·(AP)ADP resulted in a time-dependent increase in absorbance at 341 nm (Figure 3A) or 365 nm (Figure 3B), respectively. Distinct isosbestic points were observed in both cases, consistent with the formation of a single product during the reaction. Adduct formed by nonenzymic reaction of $NADP^+$ [or $N(Hx)DP^+$] and $(AP)ADP^+$ with glycolaldehyde displayed λ_{max} values of 337 and 350 nm, respectively (not shown).

Under the conditions used in Figure 3, $f_{E\cdot adduct}$ = [E·adduct]/$[E]_t$ values of 0.760 and 0.880 were calculated for reaction of E·NADP and E·(AP)ADP, respectively (see Appendix, eq 19). Use of $f_{E\cdot adduct}$ to correct the observed ΔA values (ΔA_{341nm} = 0.0348; ΔA_{365nm} = 0.0620) yielded estimates

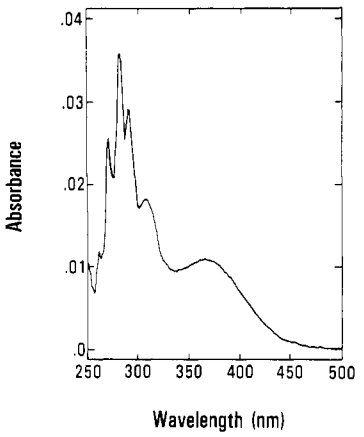

FIGURE 2: Difference spectrum (E·NADP – E) for ALR2 showing "Racker band". Tandem compartment cells (total path length, 0.9 cm) contained 17 μM ALR2 and 40 μM NADP$^+$ in MOPSE buffer, 25 °C, on the same and on the opposite sides of the partition for the sample and reference cells, respectively.

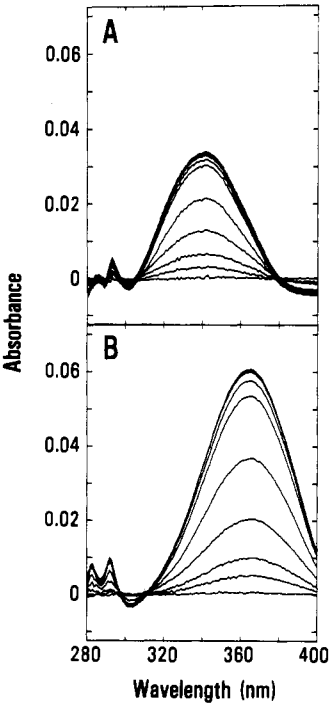

FIGURE 3: Spectrophotometric demonstration of ALR2-mediated adduct formation. Reaction mixtures contained 20 μM NADP$^+$ (panel A) or (AP)ADP$^+$ (panel B), 50 mM glycolaldehyde, and 7.5 μM ALR2 in MOPSE buffer, 15 °C. Spectra shown are difference spectra corrected for the initial difference spectrum [(sample - reference)$_t$ – (sample – reference)$_{t=0}$] measured at t = 0.07, 0.5, 1, 2, 4, 8, 12, 16, 24, and 30 min after starting the reaction by addition of glycolaldehyde. The reference cell did not contain ALR2. λ_{max} and (in parentheses) total ΔA were 341 nm (0.0348) for NADP$^+$ (panel A), and 365 nm (0.0620) for (AP)ADP$^+$ (panel B).

of ϵ_{341nm} = 6100 M^{-1} cm^{-1} and ϵ_{365nm} = 9400 M^{-1} cm^{-1} for E·NADP–ald and E·(AP)ADP–ald, respectively, that were similar to the assumed ϵ values. The ratio of these estimated values ($\epsilon_{365}/\epsilon_{341}$ = 1.51) also agreed with the ratio of slopes (1.58 ± 0.06) determined from plots of dA/dt versus [ald$_0$] for the reaction of glycolaldehyde with E·NADP and E·(AP)ADP under conditions where enolization is rate-limiting (see below) and thus the reaction rate [d[E·adduct]/dt = (dA/dt)/$\epsilon_{E\cdot adduct}$] should be identical for both nucleotides.

Fluorescence Spectra. Fluorescence properties of the E·adduct complexes are compared with those of the free and ALR2-bound reduced nucleotides in Table II. As shown, binding to ALR2 invariably caused a red shift in λ^{ex}_{max} and a blue shift in λ^{emit}_{max} and, except for NADPH, an enhancement of fluorescence yield for the bound relative to the unbound species. The fluorescence emission intensity of E·adduct was enhanced 2.3-fold and 3-fold relative to those observed for NADPH and E·NADPH, respectively. Similar results were noted for E·(AP)ADP–ald versus free (AP)ADPH or E·(AP)ADPH.

Table II: Fluorescence Properties of Free and ALR2-Bound Nucleotides and Adducts

compound or complex	relative fluorescence[a]	quenching[b] $Q_{E\cdot L}$	wavelength maxima: excitation —nm→ emission
NADPH	1.00	—	340 —118→ 458
E·NADPH	0.79	0.57	356 —98→ 454
E·NADP-ald	2.34[c]	0.70[d]	341 —80→ 421
E·NADP	—	0.45	
(AP)ADPH	0.41	—	363 —122→ 485
E·(AP)ADPH	1.15	0.52	372 —100→ 472
E·(AP)ADP-ald	2.41[c]	0.70[d]	365 —80→ 445
E·(AP)ADP	—	0.40	
(AP)ADP-ald	0.50	—	350 —113→ 463

[a] Fluorescence measured at the maximal wavelength for excitation and emission relative to $_{340}F_{458}$ = 1.00 for NADPH in MOPSE buffer, 25 °C. [b] $Q_{E\cdot L} = (F_E - F_{E\cdot L})/F_E$ for quenching of enzyme fluorescence ($_{285}F_{338}$) in MOPSE buffer, 15 °C. [c] Values normalized to [E·adduct]/[E]$_t$ = 1.00 based on $f_{E\cdot adduct}$ calculated by using eq 19 for [ald$_0$] = 50 mM. [d] Values calculated for [E·adduct]/[E]$_t$ = 1.00[c] after correction for quenching due to E·nucl and E·nucl·ald.

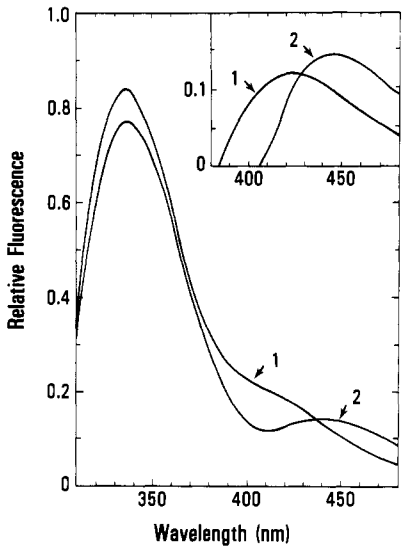

FIGURE 4: Fluorescence emission spectra for E·adduct complexes. Uncorrected emission spectra (λ^{ex} 285 nm) for E·adduct formed by reaction of glycolaldehyde with E·NADP (1) or E·(AP)ADP (2). Reaction mixtures contained 12 μM NADP$^+$ or (AP)ADP$^+$, 50 mM glycolaldehyde, and 5.0 μM ALR2 in MOPSE buffer, 25 °C. Spectra shown are for the equilibrium distribution of enzyme forms; inset shows the calculated difference spectrum (E·adduct – E·nucl) for E·NADP–ald (1; λ^{emit}_{max} 421 nm) and E·(AP)ADP–ald (2; λ^{emit}_{max} 445 nm) normalized to [E·adduct]/[E]$_t$ = 1.0 by using calculated $f_{E\cdot adduct}$ values (eq 19).

The extent of quenching ($Q_{E\cdot L}$) of the intrinsic protein fluorescence ($_{285}F_{338}$) by the bound nucleotide (Table II) was greater for NADP(H) relative to (AP)ADP(H), and increased in an order ($Q_{E\cdot NADP} < Q_{E\cdot NADPH} < Q_{E\cdot adduct}$) that paralleled the increase in binding affinity ($K_{dNADP} > K_{dNADPH} > K_{dadduct}$). The two E·adduct complexes showed similar $Q_{E\cdot adduct}$ values when corrected for quenching due to E·nucl and E·nucl·ald and normalized to $f_{E\cdot adduct}$ = 1.0.

Fluorescence energy transfer between ALR2 and bound adduct resulted in a double emission maximum (Figure 4)

Table III: Kinetic Parameters for Nonenzymic Adduct Formation[a]

parameter	nucleotide	
	$NADP^+$	$(AP)ADP^+$
k_f^{ne} (M^{-1} s^{-1})	2.1 ± 0.2	140 ± 10
k_r^{ne}[b] (s^{-1})	7.0×10^{-4}	4.0×10^{-4}
K'^{ne}_{eq} (M^{-1})	3.0×10^{3}[c]	$(3.0 \pm 0.5) \times 10^{5}$
C_{nucl} (mM)	86[d]	1.3 ± 0.1

[a] MOPSE buffer, 15 °C. See Scheme I and text for definition of parameters. [b] Calculated as k_f^{ne}/K'^{ne}_{eq}. [c] Estimated as $K'^{ne}_{eq(AP)ADP}/100$. [d] Estimated as k_k/k_f^{ne} by using k_f^{ne} measured for $NADP^+$ and k_k calculated as k_e/K_{enol} for glycolaldehyde

Table IV: Comparison of Rate Constants for Glycolaldehyde Enolization[a]

reaction	buffer	$10^8 \times k_0$ (s^{-1})	$10^6 \times k_B$[b] (M^{-1} s^{-1})
(AP)ADP–ald formation	Mops	8.5 ± 1.5	3.3 ± 0.1
E·NADP–ald formation	Mops	9.1 ± 1.0	3.2 ± 0.2
	sodium phosphate	8.4 ± 0.8	3.6 ± 0.3
iodination	sodium phosphate	7.5 ± 0.8	3.8 ± 0.2

[a] Buffer catalysis analyzed by using eq 3 for apparent k_e values measured at 15 °C, pH 7.0. [b] k_B values calculated for total [buffer].

upon excitation of the protein (λ^{ex} 285 nm), similar to that seen for the binary E·NADH complexes of several dehydrogenases (Velick, 1958). The emission intensity at 421 nm for E·NADP–ald was about 3-fold greater for excitation of the protein (285 nm) relative to excitation of the bound adduct (341 nm); a similar intensity ratio was observed for E·(AP)ADP–ald.

Scheme I

$$ald_0 \underset{k_k}{\overset{k_e}{\rightleftharpoons}} enol \underset{k_r^{ne}}{\overset{k_f^{ne}[nucl]}{\rightleftharpoons}} adduct_0$$

Nonenzymic Adduct Formation. Initial rate data were analyzed by using Scheme I, where enol is glycolaldehyde enol, nucl is oxidized nucleotide (e.g., $NADP^+$), ald_0 and $adduct_0$ are the sum of free aldehyde plus hydrate forms of glycolaldehyde and adduct, respectively,[2] k_e and k_k are the rate constants for enol formation and enol conversion back to ald_0, respectively, and k_f^{ne} and k_r^{ne} are the rate constants for adduct formation and breakdown, respectively. According to Scheme I, $v_i/[ald_0]$ (where $v_i = (dA/dt)/\epsilon_{adduct}$) should display saturation kinetics as [nucl] is increased above $C_{nucl} = k_k/k_f^{ne}$ and approach a limiting value as enol formation (k_e) becomes rate-limiting (see Appendix, eq 8). As shown in Figure 5, reaction of glycolaldehyde (50 mM) with $(AP)ADP^+$ (MOPSE buffer, 15 °C) displayed the predicted saturation kinetics. Values of k_f^{ne} and $C_{(AP)ADP}$ obtained from the fit of these data to eq 4 are listed in Table III. Because the observed rates were much lower, only k_f^{ne} could be determined for reaction of glycolaldehyde (1.0 M) with $NADP^+$ from the slope = $k_f^{ne}K_{enol}$ at low [nucl] (Figure 5). C_{NADP} was estimated from this value and k_k for glycolaldehyde (calculated as k_e/K_{enol}, see below). Buffer catalysis of k_e was analyzed by using eq 3, and the results are shown in Table IV. $N(Hx)DP^+$, which does not undergo the side reaction with glycolaldehyde observed for adenine-containing nucleotides (Grimshaw et al., 1990), gave results similar to $NADP^+$ (not shown).

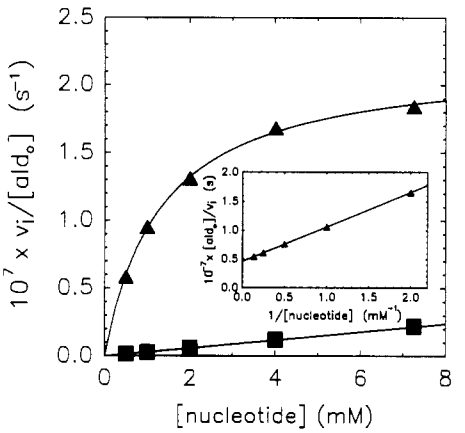

FIGURE 5: Dependence of the initial rate of nonenzymic adduct formation on [nucleotide]. Initial rates (v_i = d[adduct]/dt) were determined as described under Experimental Procedures for reaction mixtures containing the indicated concentration of nucleotide in MOPSE buffer, 15 °C. The glycolaldehyde concentration and (in parentheses) λ_{max} were 1.0 M (337 nm) for $NADP^+$ (■) and 50 mM (350 nm) for $(AP)ADP^+$ (▲). The curve for $(AP)ADP^+$ is a least-squares fit to eq 4 with 1.3 ± 0.1 mM for the apparent $K_a = C_{(AP)ADP}$ and (2.2 ± 0.1) × 10^{-7} s^{-1} for the apparent $V = k_e$. For $NADP^+$, the calculated slope = $k_f^{ne}K_{enol}$ was 3.0×10^{-6} s^{-1} M^{-1}. Inset shows a double-reciprocal plot of the $(AP)ADP^+$ data.

The equilibrium constant for (AP)ADP–ald formation[3] (K'^{ne}_{eq} = [adduct$_0$]/[(AP)ADP$^+$][enol]) was calculated from the observed ratio app K_{eq} = [adduct$_0$]/[(AP)ADP$^+$][ald$_0$] and the value of K_{enol} = [enol]/[ald$_0$], determined as described below. However, K'^{ne}_{eq} for NADP–ald formation includes an unknown contribution due to condensation of the nicotinamide side chain with the oxo group to generate a bicyclic species (Everse et al., 1971b), and was therefore estimated as $K'^{ne}_{eq(AP)ADP}/100$ on the basis of the reported difference in K_{eq} values for addition of H^- or CN^- to the 4-position of NAD^+ and $(AP)AD^+$ (Burgner & Ray, 1984b). Values of K'^{ne}_{eq} and k_r^{ne} (calculated as k_f^{ne}/K'^{ne}_{eq}) determined for $NADP^+$ and $(AP)ADP^+$ are compared in Table III.

Glycolaldehyde Enolization. When k_e was determined directly by using the chemical reaction with I_3^- to monitor the rate of enol formation (Hall & Knowles, 1975), a linear increase in k_e with [sodium phosphate] was observed. (Mops buffer reacted with I_3^- and could not be used.) Values of k_0 and k_B determined by using eq 3 are listed in Table IV. Rapid-mixing measurements of the pre-steady-state burst of I_3^- consumption at 15 °C (5 mM sodium phosphate, pH 7.0) for reaction mixtures containing 1.0 and 2.0 M glycolaldehyde gave a value of $K_{enol} \approx 1.4 \times 10^{-6}$. Prior reaction of the glycolaldehyde stock solution with 0.03% molar equiv of I_3^- had no effect on the observed burst magnitudes (Bell & Smith, 1966). Results of these studies are described in detail in the supplementary material (see paragraph at end of paper regarding supplementary material.)

Measurement of the pre-steady-state burst of E·adduct$_0$ formation by fluorescence ($_{341}F_{421}$) under conditions where k_e was rate-limiting (see below) provided a second estimate of K_{enol}. As shown in Figure 6, a burst equal to 0.10 μM E·

[2] In aqueous solution at 15 °C, glycolaldehyde exists as 4% free aldehyde; the remainder is mostly hydrate with a small amount of dimeric forms (Collins & George, 1971; Rendina et al., 1984). The adduct should be hydrated to a similar extent. Because equilibration is rapid ($t_{1/2} \approx 2.3$ s; Sorensen, 1972; Rendina et al., 1984) compared to the rates being measured, hydration has been included in the apparent k and K_{eq} values for reaction of ald_0 and $adduct_0$. Thus, k_e = true $k_e/(1 + K_{hydrate})$ and K_{enol} = true $K_{enol}/(1 + K_{hydrate})$, where $K_{hydrate}$ = [hydrate]/[aldehyde] ≈ 24, and true k_e and true K_{enol} are the k and K_{eq} values for conversion of the free aldehyde to enol, respectively. Similar expressions can be written for k'_r, k_r^{ne}, K'_{eq} and K'^{ne}_{eq}.

[3] The apparent equilibrium constant for nonenzymic adduct formation, $K'^{ne}_{eq} = (k_f^{ne}/k_r^{ne})$ = [adduct$_0$]/[enol][nucl] (units of M^{-1}), includes the concentration of hydronium ion ([H^+] = 10^{-7} M); the pH-independent constant, K_{eq}^{ne} = [adduct$_0$][H^+]/[enol][nucl], is thus equal to K'^{ne}_{eq}[H^+]. For the ALR2-mediated reaction, K'_{eq} = [E·adduct$_0$]/[enol][E·nucl] and K_{eq} = [E·adduct$_0$][H^+]/[enol][E·nucl] = K'_{eq}[H^+].

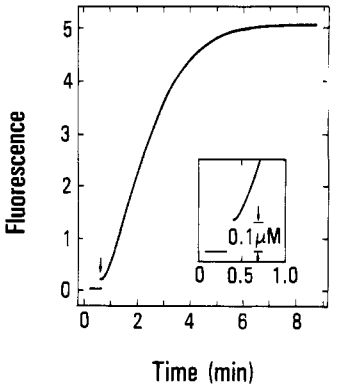

FIGURE 6: Fluorescence measurement of the pre-steady-state burst of E·adduct formation. Reaction mixture contained 20 μM $NADP^+$ and 5.0 μM ALR2 in MOPSE buffer, 15 °C. Glycolaldehyde (100 mM final concentration) was added at the arrow and the reaction was monitored by fluorescence ($_{341}F_{421}$). Inset shows the burst (0.10 μM) on an expanded scale; the value of K_{enol} = [enol]/[ald_o] estimated from these data was 1.3×10^{-6} (see text).

Scheme II

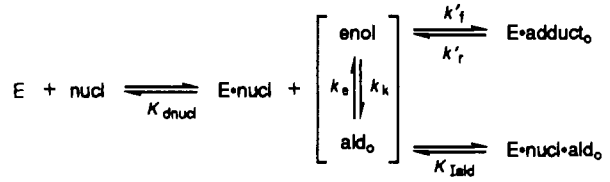

NADP–ald was detected for a reaction mixture containing 100 mM glycolaldehyde. In separate experiments, the burst magnitude was shown to be proportional to [ald_0] (50 and 100 mM) and was zero when either ALR2, $NADP^+$, or glycolaldehyde was absent. Substituting for k'_f, $f_{E\cdot NADP}$, k_e, and k_k in eq 5 (see Scheme II; [ald_0] = 100 mM, $[E]_t$ = 5 μM,

$$ald_0 \underset{k_k = 0.18\ s^{-1}}{\overset{k_e = 2.5 \times 10^{-7}\ s^{-1}}{\rightleftharpoons}} enol \xrightarrow{k'_f f_{E\cdot NADP}[E]_t = 0.56\ s^{-1}} E\cdot adduct_0 \quad (5)$$

MOPSE buffer, 15 °C) shows that, in the steady state, $[enol]_{ss} \approx 0.24\ [enol]_{eq}$. Because $[E\cdot adduct_0]_{burst} \approx [enol]_{eq} - [enol]_{ss}$ and $K_{enol} = [enol]_{eq}/[ald_0]$, we calculate that $K_{enol} \approx [E\cdot adduct_0]_{burst}/0.76[ald_0] = 1.3 \times 10^{-6}$, in good agreement with the value determined by chemical trapping with I_3^-.

Enzyme-Mediated Adduct Formation and Breakdown. Initial rate data were analyzed by using Scheme II, where E is ALR2, K_{Iald} and K_{dnucl} are the dissociation constants for release of ald_0 from E·nucl·ald_0 and release of nucl from E·nucl, respectively, k'_f is the apparent second-order rate constant for E·$adduct_0$ formation,[4] and k'_r is the apparent first-order rate constant for E·$adduct_0$ breakdown. According to Scheme II, $v_i/[ald_0]$ [where $v_i = (dA/dt)/\epsilon_{E\cdot adduct}$] should display saturation kinetics as $[E\cdot nucl]_t$ is increased above $C_{E\cdot nucl} = (k_k/k'_f)(1 + [ald_0]/K_{Iald})$ and approach a limiting value as enol formation (k_e) becomes rate-limiting (see Appendix, eq 12). As shown in Figure 7, reaction of glycolaldehyde (50 mM) with E·NADP (MOPSE buffer, 15 °C) displayed the predicted saturation kinetics. Table V lists the values of $C_{E\cdot NADP}$ and k'_f [calculated as $(k_k/C_{E\cdot NADP})(1 + [ald_0]/K_{Iald})$ by using $k_k = k_e/K_{enol}$ and K_{Iald} determined for glycolaldehyde] obtained from fits of these data to eq 4.

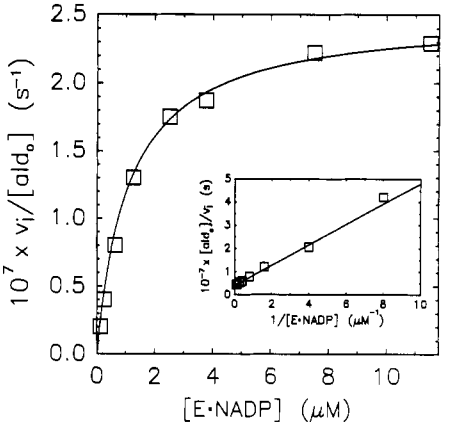

FIGURE 7: Dependence of the initial rate of ALR2-mediated E·adduct formation on [E·nucl]. Initial rates (v_i = d[E·$adduct_0$]/dt) were determined as described under Experimental Procedures by using either fluorescence ($_{285}F_{421}$) for [E·NADP] ≤ 3 μM or absorbance (λ_{max} 341 nm) for [E·NADP] ≥ 3 μM. Reaction mixtures contained 50 mM glycolaldehyde and the indicated concentration of E·NADP in MOPSE buffer, 15 °C. The curve is a least-squares fit to eq 4 with 1.1 ± 0.1 μM for the apparent $K_a = C_{E\cdot NADP}$ and (2.5 ± 0.1) × 10^{-7} s^{-1} for the apparent $V = k_e$. Inset shows a double-reciprocal plot of the same data.

Table V: Kinetic Parameters for Enzyme-Mediated Adduct Formation[a]

parameter	method	nucleotide: $NADP^+$	nucleotide: (AP)ADP^+
k'_f (M^{-1} s^{-1})	*b*	(4.9 ± 0.4) × 10^5	
	c	(6.2 ± 0.1) × 10^5	(1.6 ± 0.4) × 10^5
	d	(5.6 ± 1.0) × 10^5	(1.4 ± 0.5) × 10^5
	e	7.5 × 10^5	1.4 × 10^5
k'_r (s^{-1})	*f*	(4.7 ± 0.3) × 10^{-3}	(1.0 ± 0.1) × 10^{-3}
K'_{eq} (M^{-1})	*b*	(1.0 ± 0.1) × 10^8	
	c	(1.3 ± 0.1) × 10^8	(1.6 ± 0.4) × 10^8
	d	(1.2 ± 0.2) × 10^8	(1.4 ± 0.5) × 10^8
	e	1.6 × 10^8	1.4 × 10^8
$C_{E\cdot nucl}$ (μM)	*b*	1.1 ± 0.1	1.6[g]
K_{Iald} (mM)	*c*	25 ± 1	140 ± 30
K'_{add}	*c*	4.6 ± 0.3	32 ± 6
	d	4.2 ± 0.6	28 ± 8
	e	5.7	27

[a] MOPSE buffer, 15 °C. See Scheme II and text for definition of parameters. [b] Values obtained from fits to eq 4 of data for $v_i/[ald_0]$ versus $[E\cdot nucl]_t$. [c] Values obtained from fits to eq 4 of data for $k_{app} - k'_r$ versus [ald_0]. [d] Values determined from fits to eq 4 of fluorescence data for $f_{E\cdot adduct}$ versus [ald_0]. [e] Estimate obtained from UV–visible measurements of the stoichiometry of E·adduct formation. [f] Values determined from fits to eq 2 of the first-order fluorescence decay due to E·adduct breakdown. [g] Estimate calculated as $(k_k/k'_f)(1 + [ald_0]/K_{Iald})$ by using k_k (calculated as k_e/K_{enol}) for glycolaldehyde and the k'_f and K_{Iald} values determined from E·(AP)ADP.

Buffer catalysis of enolization by Mops and sodium phosphate was analyzed by using eq 3, and the results are shown in Table IV. As required by Schemes I and II, identical k_0 and k_B values were obtained from the variation with [Mops] of the enolization rate determined from nonenzymic production of (AP)ADP–ald_0 or from the enzyme-mediated E·NADP–ald_0 reaction. Similarly, buffer catalysis of the enolization rate by sodium phosphate was the same whether k_e was measured by trapping the enol with E·NADP or with I_3^-.

For $[E\cdot nucl]_t \ll C_{E\cdot nucl}$, the approach to equilibrium for E·$adduct_0$ formation will be a first-order process, and Scheme II predicts that the quantity $k_{app} - k'_r$, where k_{app} is the apparent first-order rate constant for this process, will display

[4] In fact, $k'_f = k_{on}k_f/(k_{off} + k_f)$, where $K_{Ienol} = k_{off}/k_{on}$ is the dissociation constant for E·nucl·enol and k_f is the *first-order* rate constant for E·nucl·enol → E·adduct. However, given $K_{enol} = 1.4 \times 10^{-6}$ and assuming $K_{Ienol} = K_a \approx 4$ M for ethylene glycol in the reverse reaction (Grimshaw et al., 1990), the fraction $f_{E\cdot nucl\cdot enol} = ([E\cdot nucl\cdot enol]/[E\cdot nucl]_t) \approx 10^{-8}$ will be negligible. Treating ALR2-mediated adduct formation as a second-order reaction is therefore analogous to comparing V/K_aE_t (units of M^{-1} s^{-1}) for an enzyme-catalyzed reaction ([A] ≪ K_a; $f_{E\cdot A} = [E\cdot A]/[E]_t \approx 0$) with k^{ne} (units of M^{-1} s^{-1}) for the nonenzymic bimolecular reaction (Schowen, 1978).

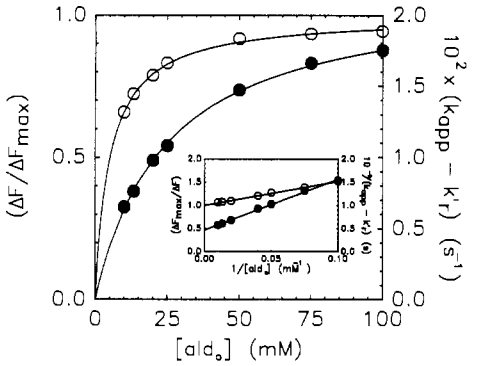

FIGURE 8: Dependence of the rate and stoichiometry of ALR2-mediated adduct formation on [glycolaldehyde]. Values of k_{app} were obtained from fits to eq 2 of the fluorescence ($_{285}F_{421}$) time course for approach to equilibrium of the reaction of glycolaldehyde with E·NADP (●). Reaction mixtures contained 20 μM $NADP^+$, 0.125 μM ALR2, and the indicated concentration of glycolaldehyde in MOPSE buffer, 15 °C. The experimental k_{app} values were corrected for the contribution of k'_r (0.0047 s^{-1}); the curve is a least-squares fit to eq 4 with 25 ± 1 mM for the apparent $K_a = K_{Iald}$ and 0.022 ± 0.001 s^{-1} for the apparent $V = k'_f K_{enol} K_{Iald}$. Also plotted are $f_{E\cdot adduct}$ values estimated for the same reaction mixtures as $\Delta F/\Delta F_{max}$ at equilibrium (○). Least-squares analysis (eq 4) gave 4.8 ± 0.7 mM for the apparent $K_a = K_{Iald}/(1 + K'_{add})$. Inset shows a double-reciprocal plot of the same data.

saturation kinetics as $[ald_0]$ is increased above K_{Iald} and approach a maximum of $k'_f K_{enol} K_{Iald}$ (see Appendix, eq 16). In Figure 8, $k_{app} - k'_r$ for E·NADP–ald_0 formation shows the predicted saturation behavior; similar results were obtained for E·(AP)ADP–ald_0 formation (not shown). The K_{Iald} and k'_f values determined from fits of the data to eq 4 are listed in Table V.

The k'_r values were determined directly from the first-order decay of fluorescence due to E·$adduct_0$ breakdown [$_{341}F_{421}$ and $_{285}F_{445}$ for E·NADP–ald_0 and E·(AP)ADP–ald_0, respectively]; plots of log $(1 - \Delta F/\Delta F_{max})$ versus time were in all cases linear through 4 half-lives (not shown). The observed k'_r values [obtained from fits to eq 2 and corrected for a small (<10%) contribution due to k'_f at $[ald_0]$ = 0.5 mM] are listed in Table V.

Figure 8 also shows a plot of $[ald_0]$ versus $\Delta F/\Delta F_{max}$ at equilibrium, which is equivalent to $f_{E\cdot adduct}$. According to Scheme II, the apparent half-saturation constant for $[ald_0]$ in this case will be $K_{Iald}/(1 + K'_{add})$, where K'_{add} = [E·adduct$_0$]/[E·nucl·ald_0] is the apparent equilibrium constant for adduct formation at the ALR2 active site (see Appendix, eq 19). When fitted to eq 4, the data in Figure 8 gave an apparent K_a = 4.8 ± 0.7 mM; similar data for E·(AP)ADP–ald_0 gave a value of 4.9 ± 1.0 mM. The K'_{add} values derived from these data [as $1 - (K_{Iald}/\text{app } K_a)$] are compared in Table V with the K'_{add} values determined by direct measurement of the extent of adduct formation by using UV–visible spectroscopy (cf. Figure 3), and by calculation (as app V/k'_r) with the app V obtained from the plot of $k_{app} - k'_r$ versus $[ald_0]$ (cf. Figure 8).

The equilibrium constant for E·adduct formation[3] (K'_{eq} = [E·$adduct_0$]/[E·nucl][enol]) was estimated by several methods: (1) as k'_f/k'_r, with k'_r measured directly and k'_f determined from $v_i/[ald_0]$ versus $[E_{nucl}]_t$ (cf. Figure 7) or $k_{app} - k'_r$ versus $[ald_0]$ (cf. Figure 8); or (2) as $K'_{eq} = (K'_{add}/K_{enol}K_{Iald})$, with the K'_{add} value obtained from the dependence of $f_{E\cdot adduct}$ on $[ald_0]$ (cf. Figure 8) or from UV–visible measurements (cf. Figure 3). The latter values, which are based on equilibrium rather than rate measurements, were also used to estimate k'_f (as $K'_{eq}k'_r$). The various K'_{eq} and k'_f values thus obtained for $NADP^+$ and $(AP)ADP^+$ are compared in Table V.

Discussion

Spectral Analysis and Structural Interpretation. Reaction of glycolaldehyde with E·NADP produced a chromophore absorbing maximally at 341 nm (Figure 3A), consistent with the formation of a 1,4-dihydro-4-(1-hydroxy-2-oxoethyl)-nicotinamide structure (I) analogous to that determined by ^1H NMR for the adduct produced by reaction of pyruvate with NAD (II) bound at the lactate dehydrogenase active site (Arnold & Kaplan, 1974). However, the fluorescence displayed by the E·NADP–ald and E·(AP)ADP–ald adduct complexes with ALR2 appears to be unique.

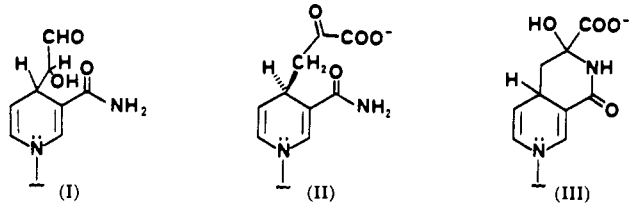

Pyruvate adduct formation with $NAD(P)^+$ yields fluorescent products but only *after* condensation of the 2-oxo group with the 3-acetamido moiety has occurred to give a bicyclic species (III) (Everse et al., 1971b). Structures that do not undergo cyclization, such as (AP)AD–pyruvate (DiSabato, 1968) and the NAD–oxime adducts (Torreilles et al., 1983), do not fluoresce. Weak fluorescence was observed for a reaction mixture containing the binary E·NAD–pyruvate complex with lactate dehydrogenase (Griffin & Criddle, 1970), but not for excitation at λ^{ex}_{max} (325 nm) for the enzyme-bound adduct (Everse et al., 1971a,b).[5]

As shown in Table II, the fluorescence properties of the binary E·NADP–ald complex are distinct from those of either NADPH or E·NADPH, indicating that the absorbance and fluorescence changes do not arise from simple reduction of E·NADP. Thus, λ^{ex}_{max} for E·NADP–ald is blue-shifted 15 nm relative to E·NADPH, while λ^{emit}_{max} is blue-shifted 37 nm relative to free NADPH and 33 nm relative to E·NADPH.

Comparison of II with the proposed structure for (AP)-ADP–ald (IV) suggests a possible rationale for the unique fluorescence of I and IV. The oxo group in IV is an aldehyde, while in II it is a ketone adjacent to a carboxylate (ionized at pH 7). On the basis of hydration data for glycolaldehyde (Gruen & McTigue, 1963; Collins & George, 1971) and pyruvate (Sugrobova et al., 1974), IV and II should consist of about 4% and 94% free carbonyl form, respectively. Hydration of IV to give V thus appears to serve the same purpose as cyclization of II to give III, namely, to change an sp^2-hybridized carbonyl moiety to an sp^3-hybridized or carbinolamine, respectively. The lack of fluorescence by the NADP–oxime adducts is consistent with this idea (Torreilles et al., 1983).

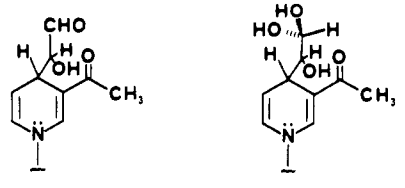

[5] Fluorescence was detected for excitation at λ_{max} of the bicyclic structure III ($_{345}F_{430}$) and at 388 nm ($_{390}F_{448}$); the latter absorbance band, seen for E·NAD–pyruvate (388 nm) and E·(AP)AD–pyruvate (410 nm), has been attributed to either a charge transfer complex or formation of an imino bond (Griffin & Criddle, 1970).

Several lines of evidence point to a strong interaction of nucleotides with the ALR2-binding site, notably the fact that ALR2 will bind *both* $NADP^+$ and NADPH with K_d values less than 0.1 μM (Table I). The broad absorption band at 366 nm (or "Racker band") detected for the binary E·NADP complex of ALR2 (Figure 2) has also been observed for the binary E·NAD(P) complexes of glyceraldehyde-3-phosphate dehydrogenase (Racker & Krimsky, 1952) and dihydrofolate reductase (Neef & Huennekens, 1975), two enzymes that, like ALR2, display unusually tight binding of the oxidized nucleotide cofactor [K_{dNAD} = 0.06 μM for rabbit glyceraldehyde-3-phosphate dehydrogenase (Velick, 1958); K_{dNADP} = 0.74 μM for human dihydrofolate reductase (Prendergast et al., 1989)]. With regard to the latter enzyme, we recently presented evidence for a close similarity of the NADP(H) binding domains of ALR2 and dihydrofolate reductase, based on an analysis of the predicted secondary structure for bovine lens ALR2 (Schade et al., 1990).

The red shift of λ^{ex}_{max} seen when NADPH and (AP)ADPH are bound to ALR2 (Table II) is consistent with the red shift of the absorbance λ_{max} seen for the binary E·NADPH complex of ALR2 isolated from rabbit muscle (Cromlish & Flynn, 1983) and pig lens (Branlant, 1982), and for the closely related enzyme aldehyde reductase, isolated from human (Wermuth et al., 1977) and pig (Flynn et al., 1975) tissues. Although the molecular basis for these shifts is not known, Cromlish and Flynn (1983) have noted that ALR2 and aldehyde reductase are rather unique in this regard, since Fisher et al. (1969) correlated a red-shifted λ_{max} for E·NAD(P)H with "B-side" (*pro-S*) specificity for NAD(P)H oxidation, while ALR2 (Walton, 1973) and aldehyde reductase (Flynn et al., 1975) are both "A-side" (*pro-R*) specific enzymes. The quenching of NADPH fluorescence in the binary E·NADPH complex with ALR2 is also unusual; most dehydrogenases, with the exception of glyceraldehyde-3-phosphate dehydrogenase (Velick, 1958), show enhanced fluorescence for bound NAD(P)H.

Binding to ALR2 caused a red shift in λ^{ex}_{max} for (AP)ADP–ald similar to that seen for E·NADPH and E·(AP)ADPH (Table II). Yet, the apparent red shift for E·NADP–ald was much less. As noted above, NAD–pyruvate can cyclize to generate III (λ_{max} 340 nm) in solution (Ozols & Marinetti, 1969; DiSabato, 1970; Everse et al., 1971a,b; Arnold & Kaplan, 1974), whereas only structure II can form (λ_{max} 325 nm) at the lactate dehydrogenase active site (Gutfreund et al., 1968; Griffin & Criddle, 1970; Sugrobova et al., 1972; Burgner & Ray, 1974). Similarly, λ_{max} for a series of bicyclic NAD–ketone adducts is 15–17 nm higher than λ_{max} for the corresponding NAD–oxime structures, which do not undergo cyclization (Torreilles et al., 1983). The observed λ_{max} for E·NADP–ald (341 nm) thus probably represents a red shift of ≥19 nm from the λ_{max} estimated for the monocyclic adduct I (322 nm).

Kinetic Analysis and Mechanistic Interpretation. As detailed under Results, the kinetic behavior of the nonenzymic and ALR2-mediated adduct formation reactions were fully consistent with the mechanisms shown in Schemes I and II, respectively. In each case, the reaction was first-order in [ald_0] and [nucl] (or [E·nucl]$_t$) at low concentrations of the latter where enol formation is in rapid equilibrium. Both the nonenzymic (Figure 5) and enzyme-mediated (Figure 7) reactions displayed saturation kinetics as [nucl] or [E·nucl]$_t$, respectively, was increased and enol formation became rate-limiting. Saturation kinetics observed for [ald_0] in the enzyme-mediated reaction, under conditions where enol formation is in rapid equilibrium (Figure 8), are readily explained by the competition of enol and ald_0 for the available E·nucl.

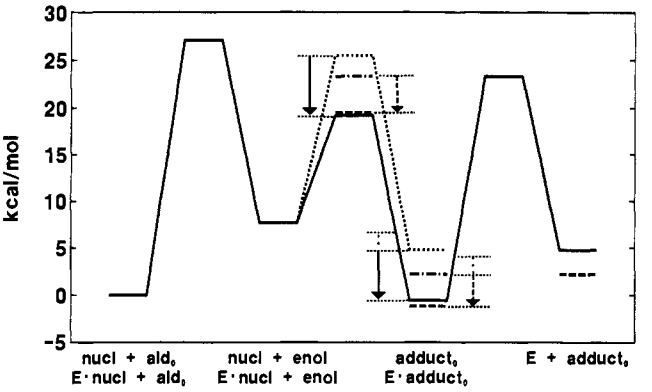

FIGURE 9: Free energy diagram comparing nonenzymic and ALR2-mediated adduct formation. Standard states are [E·nucl]$_t$ = [nucl]$_t$ = 1.0 M and [ald_0] = 50 mM at pH 7.0, 15 °C. Results are compared for the nonenzymic (···) and ALR2-mediated (—) reactions with $NADP^+$ and for the nonenzymic (·-·) and ALR2-mediated (---) reactions with (AP)ADP^+. The first transition state (enol formation, $k_e = 2.5 \times 10^{-7}$ s^{-1}) is common to all reactions. The second transition state is for adduct$_0$ formation (k_f^{ne} and $f_{E\cdot nucl}k'_f$) and breakdown (k_r^{ne} and k'_r), and the third is for dissociation of ALR2-bound adduct$_0$ (k_{off}). The arrows show $\Delta\Delta G^{\ddagger} = (\Delta G^{\ddagger}_{E\cdot adduct} - \Delta G^{\ddagger}_{adduct})$ for enhancement of the *rate* of adduct$_0$ formation at the ALR2 active site and $\Delta\Delta G' = (\Delta G'_{E\cdot adduct} - \Delta G'_{adduct})$ for stabilization of enzyme-bound adduct$_0$ for $NADP^+$ (→) and (AP)ADP^+ (-·→); the extension shown for $\Delta\Delta G'$ (···) reflects an additional −1.8 kcal/mol stabilization by the enzyme should E·adduct$_0$ be unhydrated.[2] See text and Tables III and V for definitions and values of individual rate and equilibrium constants.

Two additional lines of evidence implicate glycolaldehyde enol as the reactant in adduct formation. First, an identical dependence on buffer concentration (Mops or sodium phosphate) was observed for the limiting rate constant (k_e) measured for nonenzymic (AP)ADP–ald formation, ALR2-mediated E·NADP–ald formation, and chemical trapping of the enol via iodination (Table IV). Second, the value of K_{enol} determined from the pre-steady-state burst of E·NADP–ald formation (Figure 6) corresponded closely with the value estimated by rapid-mixing kinetics using the iodination trapping method. The good agreement observed for the k'_f, K'_{eq}, and K'_{add} values determined by both equilibrium and kinetic measurements (Table V) further supports the validity of Scheme II.

To illustrate the results we have obtained, we summarize the kinetic and thermodynamic constants measured here in the free energy diagram shown in Figure 9. Inspection of Figure 9 reveals that the diagram is in accord with Schemes I and II. For the standard state chosen ([ald_0] = 50 mM; [nucl] = [E·nucl]$_t$ = 1.0 M), the transition state for enol formation limits the overall rate of either reaction. The change in rate-limiting step occurs when [nucl] = C_{nucl} and [E·nucl]$_t$ = $C_{E\cdot nucl}$, at which point the transition states for enol formation and adduct formation become equal in energy.[6] For example, the 7.9 kcal/mol difference between $\Delta G^{\ddagger}$ for k_e (27.1 kcal/mol) and $\Delta G^{\ddagger}$ for E·NADP–ald formation (19.2 kcal/mol) is reduced to zero when [E·NADP]$_t$ is decreased 10^6-fold from a standard state of 1.0 M to the $C_{E\cdot NADP}$ value of 1.1 μM.

According to Jencks (1981), the difference between $\Delta G^{\ddagger}$ for the nonenzymic reaction and $\Delta G^{\ddagger}$ for ALR2-mediated adduct$_0$ formation can be attributed to utilization of the intrinsic binding energy of the nucleotide and glycolaldehyde

[6] Because k_e is the same in both cases, C_{nucl} and $C_{E\cdot nucl}$ directly determine the rate enhancement by ALR2: $(C_{E\cdot nucl}/C_{nucl})^{-1} = \exp[(\Delta G^{\ddagger}_{E\cdot adduct} - \Delta G^{\ddagger}_{adduct})/RT]$.

enol to lower the activation energy barrier for adduct formation. The enzyme presumably accomplishes this by using this binding energy to increase the concentration of encounter complexes at the active site in which the two molecules possess the correct geometry to react without the loss of entropy that otherwise must occur for the bimolecular reaction in solution. Since the adduct is essentially a bisubstrate analogue, a similar effect can explain the difference in $\Delta G'$ for adduct$_0$ formation. Thus, the intrinsic binding energy of the aldehyde portion of the adduct structure can be utilized to stabilize the reaction product at the ALR2 active site relative to that in solution.

On the basis of the results shown in Figure 9 for (AP)ADP$^+$, the effects of the enzyme on the transition state for adduct formation ($\Delta\Delta G^\ddagger$ = −3.8 kcal/mol) and on K_{eq} for the reaction ($\Delta\Delta G'$ = −3.4 kcal/mol) appear to be similar.[7] However, $\Delta\Delta G^\ddagger$ and $\Delta\Delta G'$ for NADP$^+$ were 2.6 and 2.0 kcal/mol more negative than the corresponding values for (AP)ADP$^+$, and thus there must be some additional interaction with the enzyme that is specific for NADP$^+$. In other words, the ratio of k_f values for the two nucleotides has switched from 66-fold in favor of reaction with (AP)ADP$^+$ in solution to 3-fold in favor of NADP$^+$ at the enzyme active site,[8] corresponding to a 200-fold overall change in relative reactivity. K'_{add}, the apparent equilibrium constant for adduct formation from *bound* aldehyde and nucleotide, displayed a similar effect. Thus, K'_{add} for (AP)ADP–ald$_0$ formation was only 5.6-fold greater than K'_{add} for NADP–ald$_0$ (Table V), compared with a predicted 100-fold preference for reaction with the 3-acetylpyridine analogue on the basis of K_{eq} values measured for CN^- and H^- addition to (AP)AD$^+$ and NAD$^+$ (Burgner & Ray, 1984a).

As an alternative to the approach of Jencks, the additional stability of E·NADP–ald$_0$ relative to E·(AP)ADP–ald$_0$ can be rationalized in terms of a differential "chelate effect" (Ray & Long, 1976) for binding of these bisubstrate analogues at the ALR2 active site. From the relationship

$$\begin{array}{ccc} \text{E + nucl + enol} & \xrightleftharpoons{K'^{ne}_{eq}} & \text{E + adduct}_o \\ \Big\| K_{dnucl} & & \Big\| K_{dadduct} \\ \text{E·nucl + enol} & \xrightleftharpoons{K'_{eq}} & \text{E·adduct}_o \end{array} \qquad (6)$$

we calculate a value of 2×10^{-12} M for $K_{dNADP\text{-}ald} = K'^{ne}_{eq} K_{dNADP}/K'_{eq}$. A similar calculation for (AP)ADP$^+$ yields $K_{d(AP)ADP\text{-}ald} = 5 \times 10^{-10}$ M. If we divide the $K_{dadduct}$ value into the product $K_{dnucl}K_{lald}$, essentially comparing the sequential binding of nucl and ald with the binding of adduct, the resultant value for NADP–ald$_0$ (1000) is 15-fold greater than the value calculated for (AP)ADP–ald$_0$ (67). Combining this with the factor of 5.6 from the ratio of K'_{add} values discussed above, we can account for 84% of the 100-fold difference in K_{eq} predicted from model studies.

Regardless of the rationale used, the major portion of the energetic advantage for NADP$^+$ over (AP)ADP$^+$ appears to be expressed only when both substrates are bound. Thus, $K_{dNADP(H)}$ is only 3–8-fold lower than $K_{d(AP)ADP(H)}$ (Table I), compared with a predicted 15–200-fold ratio if the full energy difference was utilized to enhance the binding affinity in the binary E·nucl(H) complex. For NADP$^+$, the values shown in Figure 9 for $\Delta\Delta G^\ddagger$ (−6.4 kcal/mol) and $\Delta\Delta G'$ (−5.4 to −7.2 kcal/mol[7]) correspond to a 79 000-fold enhancement of the forward reaction rate and a 13 000–320 000-fold stabilization of adduct at the ALR2 active site relative to the reaction in solution.

Finally, we ask whether k'_r corresponds to reversal of adduct formation, as shown in Scheme II, or to release of adduct from E·adduct. Because k_{off} for dissociation of E·adduct cannot be greater than k'_r (10^{-3} s^{-1}) and $K_{dadduct} = k_{off}/k_{on}$, we can calculate that k_{on} must be $\leq 2 \times 10^6$ M^{-1} s^{-1}, which is comparable to the rate constant measured for association of NADPH with *Escherichia coli* dihydrofolate reductase (Cayley et al., 1981). Assuming that k_{on} for NADP–ald is similar and using the $K_{dNADP\text{-}ald}$ value determined above, we calculate that k_{off} for dissociation of E·NADP–ald must be $\leq 4 \times 10^{-6}$ s^{-1}. As shown in Figure 9, this corresponds to a 3.9 kcal/mol difference in $\Delta G^\ddagger$ for k'_r versus k_{off}, and thus k'_r for E·NADP–ald must represent the reverse reaction to give E·nucl plus enol. Furthermore, because k_{off} for adduct is low catalysis by the enzyme of the *overall* adduct formation reaction relative to the nonenzymic process[9] is at most 67-fold for NADP–ald. The rate of dissociation and of adduct breakdown may be comparable for E·(AP)ADP–ald.

Acknowledgments

We thank Ms. Guiti Jahangiri for purification of bovine kidney aldose reductase and Ms. Sue Burke for assistance with the manuscript preparation.

Appendix

Kinetic Analysis of Nonenzymic Adduct Formation. Equation 7 describes the initial rate of nonenzymic adduct formation for Scheme I:

$$v_i = d[\text{adduct}_0]/dt = k_e[\text{ald}_0][\text{nucl}]/(k_k/k_f^{ne} + [\text{nucl}]) \qquad (7)$$

Because the reaction is first-order in [ald$_0$] under all conditions

$$v_i/[\text{ald}_0] = k_e[\text{nucl}]/(k_k/k_f^{ne} + [\text{nucl}]) \qquad (8)$$

where eq 8 has the same form as the Michaelis–Menten equation:

$$v_i = VA/(K_a + A) \qquad (4)$$

with $v_i = v_i/[\text{ald}_0]$, A = [nucl], $V = k_e$, and $K_a = k_k/k_f^{ne}$. For statistical analysis, $v_i/[\text{ald}_0]$ values as a function of [nucl] are fitted to eq 4, while in double-reciprocal form

$$[\text{ald}_0]/v_i = 1/k_e + (1/[\text{nucl}])(1/k_f^{ne}K_{enol}) \qquad (9)$$

Equation 9 is better suited to graphical analysis, since the ordinate intercept ($1/k_e$) and slope ($1/k_f^{ne}K_{enol}$) obtained from a plot of $[\text{ald}_0]/v_i$ versus $1/[\text{nucl}]$ are strictly analogous to $1/V$ and K_a/V obtained from a Lineweaver–Burk plot of $1/v_i$ versus $1/A$. Thus, $v_i/[\text{ald}_0]$ (units of s^{-1}) for nonenzymic adduct formation will display saturation by [nucl], changing from a *pseudo*-first-order reaction [i.e., $(V/K_a)A = k_f^{ne}K_{enol}[\text{nucl}]$] to a *pseudo*-zero-order reaction (i.e., $V = k_e$). The apparent half-saturation constant for nucleotide (k_k/k_f^{ne}) is designated

[7] $\Delta\Delta G'$ can be up to 1.8 kcal/mol lower depending on the hydration of E·adduct.[2]

[8] The relative reactivity ratio varies with [ald$_0$] due to the difference in K_{lald} values, ranging from 3.7 = $(k'_f f_{E\cdot NADP}/k'_f f_{E\cdot(AP)ADP})$ for [ald$_0$] ≪ 25 mM to 0.67 = $(k'_f f_{E\cdot NADP}/k'_f f_{E\cdot(AP)ADP})(K_{lald(NADP)}/K_{lald[(AP)ADP]})$ for [ald$_0$] ≫ 140 mM.

[9] The maximum catalytic effect for turnover (i.e., E·nucl + ald$_0$ → E + adduct$_0$) will occur when enol formation is rapid and the enzyme is not saturated (Schowen, 1978), where both the nonenzymic and ALR2-mediated reactions are first-order in [ald$_0$] and [nucl]$_t$ (or [E·nucl]$_t$). The ratio of rate constants calculated for [NADP$^+$]$_t$ = [E·NADP]$_t$ ≪ $C_{E\cdot NADP}$ and [ald]$_0$ = 50 mM is then $[k'_r f_{E\cdot NADP} k_{off}/(k'_r + k_{off})]/k_f^{ne}$.

C_{nucl} by analogy to the "reverse commitment to catalysis" (C_r) used to describe enzymic mechanisms (Northrop, 1977). Like a standard C_r, C_{nucl} expresses the tendency of enol to return to ald versus the forward reaction to give adduct. For [nucl] = C_{nucl}, enol partitions equally in both directions.

Kinetic Analysis of Enzyme-Mediated Adduct Formation. Equation 10 describes the initial rate of enzyme-mediated adduct formation for Scheme II:

$$v_i = d[E\cdot adduct_0]/dt = k_e[ald_0][E\cdot nucl]/(k_k/k'_f + [E\cdot nucl]) \quad (10)$$

However, because E·nucl must partition between E·adduct$_0$ and E·nucl·ald$_0$, the factor

$$f_{E\cdot nucl} = [E\cdot nucl]/[E]_t = 1/(1 + K_{dnucl}/[nucl] + [ald_0]/K_{lald}) \quad (11)$$

must be included, where $K_{dnucl} = [E][nucl]/[E\cdot nucl]$ and $K_{lald} = [E\cdot nucl][ald_0]/[E\cdot nucl\cdot ald_0]$. For [nucl] $\gg K_{dnucl}$, the second term in eq 11 can be ignored and $[E\cdot nucl]_t = [E\cdot nucl] + [E\cdot nucl\cdot ald_0]$ can be substituted for $[E]_t$. The modified rate equation

$$v_i/[ald_0] = k_e[E\cdot nucl]_t/\{(k_k/k'_f)(1 + [ald_0]/K_{lald}) + [E\cdot nucl]_t\} \quad (12)$$

again has the form of eq 4 with $v_i = v_i/[ald_0]$, $A = [E\cdot nucl]_t$, $V = k_e$, and $K_a = (k_k/k'_f)(1 + [ald_0]/K_{lald})$, or in double-reciprocal form

$$[ald_0]/v_i = (1/k_e) + (1/k'_f K_{enol})(1 + [ald_0]/K_{lald})(1/[E\cdot nucl]_t) \quad (13)$$

Thus, at constant $[ald_0]$, $v_i/[ald_0]$ for enzyme-mediated adduct formation will display saturation by $[E\cdot nucl]_t$, changing from a *pseudo*-first-order reaction [i.e., $(V/K_a)A = k'_f K_{enol}[E\cdot nucl]_t/(1 + [ald_0]/K_{lald})$] to a *pseudo*-zero-order reaction (i.e., $V = k_e$). At this point, $v_i/[ald_0]$ for the enzyme-mediated and nonenzymic reactions must become equal, since both are limited by the rate of enol formation. The apparent half-saturation constant for $[E\cdot nucl]_t$, $C_{E\cdot nucl} = (k_k/k'_f)(1 + [ald_0]/K_{lald})$, again expresses the tendency of enol to return to ald$_0$ versus reaction forward to give E·adduct$_0$.

For $[E\cdot nucl]_t \ll C_{E\cdot nucl}$, enzyme-mediated adduct formation is first-order in $[E\cdot nucl]_t$ and one can measure either the initial rate or the rate of approach to equilibrium. In the latter case, Scheme II can be described by the integrated rate law:

$$\ln\{[E\cdot adduct_0]_\infty/([E\cdot adduct_0]_\infty - [E\cdot adduct_o]_t)\} = k_{app}t \quad (14)$$

where k_{app}, the *pseudo*-first-order rate constant for approach to equilibrium

$$k_{app} = k'_f K_{enol}[ald_0]f_{E\cdot nucl} + k'_r \quad (15)$$

includes k'_r, the rate constant for E·adduct$_0$ decomposition. (k_{app} can be considered a *pseudo*-first-order rate constant because [enol] and $[ald_0]$ are in rapid equilibrium and $\Delta[ald_0]/[ald_0]_{t=0} \approx 0$.) Substituting for $f_{E\cdot nucl}$ and rearranging, we obtain

$$k_{app} - k'_r = k'_f K_{enol} K_{lald}[ald_0]/(K_{lald} + [ald_0]) \quad (16)$$

Equation 16 has the same form as eq 4 with $v_i = k_{app} - k'_r$, $A = [ald_0]$, $V = k'_f K_{enol} K_{lald}$, and $K_a = K_{lald}$. Thus, $k_{app} - k'_r$ (i.e., the net contribution of adduct *formation* to k_{app}) will display saturation by $[ald_0]$ with an apparent half-saturation constant equal to K_{lald} and a maximum value of $k'_f K_{enol} K_{lald}$, or in double-reciprocal form

$$1/(k_{app} - k'_r) = (1/k'_f K_{enol} K_{lald}) + (1/[ald_0])(1/k'_f K_{enol}) \quad (17)$$

Provided k'_r can be measured independently, analysis of the k_{app} values then allows determination of K_{lald} and k'_f (i.e., calculated as app $V/K_{lald}K_{enol}$).

We now define a new parameter, K'_{add}, based on the equation

$$E\cdot nucl\cdot ald_0 \overset{K_{lald}}{\rightleftharpoons} E\cdot nucl + ald_0 \overset{K_{enol}}{\rightleftharpoons} E\cdot nucl + enol \overset{K'_{eq}}{\rightleftharpoons} E\cdot adduct_0 \quad (18)$$

where $K'_{add} = K_{lald}K_{enol}K'_{eq}$ is the apparent equilibrium constant for adduct formation at the active site ($K'_{add} = [E\cdot adduct_0]/[E\cdot nucl\cdot ald_0]$). The equation

$$f_{E\cdot adduct} = [E\cdot adduct_0]/[E\cdot nucl]_t = K'_{add}/(1 + K'_{add} + K_{lald}/[ald_0]) \quad (19)$$

or in double-reciprocal form

$$(1/f_{E\cdot adduct}) = (1 + 1/K'_{add}) + (1/[ald]_0)(K_{lald}/K'_{add}) \quad (20)$$

predicts that $f_{E\cdot adduct}$ will approach a maximum of $K'_{add}/(1 + K'_{add})$ as $[ald_0]$ is increased above an apparent half-saturation level equal to $K_{lald}/(1 + K'_{add})$. In other words, the apparent dissociation constant for ald$_o$ release from $[E\cdot nucl\cdot ald_0]_t = [E\cdot nucl\cdot ald_0] + [E\cdot adduct_0]$ is decreased by the factor $1 + K'_{add}$ due to adduct formation. The variation of $f_{E\cdot adduct}$ as a function of $[ald_0]$ thus provides an independent estimate of K'_{add} and therefore K'_{eq}. (K'_{add} can also be estimated as app V/k'_r by using the apparent V obtained from the dependence of $k_{app} - k'_r$ on $[ald_0]$, because app $V/k'_r = k'_f K_{enol} K_{lald}/k'_r = K_{enol}K_{lald}K'_{eq} = K'_{add}$.)

Supplementary Material Available

Supplementary figures (S1 and S2) and experimental procedures and results for measurement of K_{enol} and determination of sodium phosphate buffer catalysis of k_e by using I_3^- (3 pages). Ordering information is given on any current masthead page.

References

Alberty, R. A., & Koerber, B. M. (1957) *J. Am. Chem. Soc. 79*, 6379.

Arnold, L. J., Jr., & Kaplan, N. O. (1974) *J. Biol. Chem. 249*, 652–655.

Awtrey, A. D., & Connick, R. E. (1951) *J. Am. Chem. Soc. 73*, 1842–1843.

Bell, R. P., & Smith, P. W. (1966) *J. Chem. Soc. B*, 241–243.

Bio-Rad Laboratories (1986) Bio-Rad Technical Bulletin 2020, Bio-Rad Laboratories, Richmond, CA.

Branlant, G. (1982) *Eur. J. Biochem. 129*, 99–104.

Burgner, J. W., II, & Ray, W. J., Jr. (1974) *Biochemistry 13*, 4229–4237.

Burgner, J. W., II, & Ray, W. J., Jr. (1978) *Biochemistry 17*, 1654–1661.

Burgner, J. W., II, & Ray, W. J., Jr. (1984a) *Biochemistry 23*, 3620–3626.

Burgner, J. W., II, & Ray, W. J., Jr. (1984b) *Biochemistry 23*, 3636–3648.

Burgner, J. W., II, Ainslie, G. R., Jr., Cleland, W. W., & Ray, W. J., Jr. (1978) *Biochemistry 17*, 1646–1653.

Burton, R. M., & Kaplan, N. O. (1954) *J. Biol. Chem. 206*, 283–297.

Burton, R. M., San Pietro, A., & Kaplan, N. O. (1957) *Arch. Biochem. Biophys. 70*, 87–107.

Cayley, R. J., Dunn, S. M. J., & King, R. W. (1981) *Biochemistry 20*, 874–879.
Cleland, W. W. (1979) *Methods Enzymol. 63*, 103–138.
Collins, G. C. S., & George, W. O. J. (1971) *J. Chem. Soc. B*, 1352–1355.
Cromlish, J. A., & Flynn, T. G. (1983) *J. Biol. Chem. 258*, 3416–3424.
DiSabato, G. (1968) *Biochem. Biophys. Res. Commun. 33*, 688–695.
DiSabato, G. (1970) *Biochemistry 9*, 4594–4600.
Everse, J., Barnett, R. E., Thorne, C. J. R., & Kaplan, N. O. (1971a) *Arch. Biochem. Biophys. 143*, 444–460.
Everse, J., Zoll, E. C., Kahan, L., & Kaplan, N. O. (1971b) *Bioorg. Chem. 1*, 207–233.
Fisher, H. F., Adija, D. L., & Cross, D. G. (1969) *Biochemistry 8*, 4424–4430.
Flynn, T. G., Shires, J., & Walton, D. (1975) *J. Biol. Chem. 250*, 2933–2940.
Griffin, J. H., & Criddle, R. S. (1970) *Biochemistry 9*, 1195–1205.
Grimshaw, C. E., Shahbaz, M., Jahangiri, G., Putney, C. G., McKercher, S. R., & Mathur, E. J. (1989) *Biochemistry 28*, 5343–5353.
Grimshaw, C. E., Shahbaz, M., & Putney, C. G. (1990) *Biochemistry* (following paper in this issue).
Gruen, L. C., & McTigue, P. T. (1963) *J. Chem. Soc.*, 5217–5229.
Gutfreund, H., Cantwell, R., McMurray, C. H., Criddle, R. S., & Hathaway, G. (1968) *Biochem. J. 106*, 683–687.
Hall, A., & Knowles, J. R. (1975) *Biochemistry 14*, 4348–4352.
Jencks, W. P. (1981) *Proc. Natl. Acad. Sci. U.S.A. 78*, 4046–4050.
Kador, P. F., Robison, W. G., & Kinoshita, J. H. (1985) *Annu. Rev. Pharmacol. Toxicol. 25*, 691–714.
McKercher, S. R., Mathur, E. J., & Grimshaw, C. E. (1985) *Fed. Proc. 44*, 427.
Neef, V. M., & Huennekens, F. M. (1975) *Arch. Biochem. Biophys. 171*, 435–443.
Northrop, D. B. (1977) in *Isotope Effects on Enzyme-Catalyzed Reactions* (Cleland, W. W., O'Leary, M. H., & Northrop, D. B., Eds.) pp 122–152, University Park Press, Baltimore, MD.
Orr, G. A., & Blanchard, J. S. (1984) *Anal. Biochem. 142*, 232–234.
Ozols, R. F., & Marinetti, G. V. (1969) *Biochem. Biophys. Res. Commun. 34*, 712–718.
Prendergast, N. J., Appleman, J. R., Delcamp, T. J., Blakley, R. L., & Freisheim, J. H. (1989) *Biochemistry 28*, 4645–4650.
Racker, E., & Krimsky, I. (1952) *J. Biol. Chem. 198*, 731–743.
Ray, W. J., Jr., & Long, J. W. (1976) *Biochemistry 15*, 4018–4028.
Rendina, A. R., Hermes, J. D., & Cleland, W. W. (1984) *Biochemistry 23*, 5148–5156.
Schade, S. Z., Early, E. R., Williams, R. T., Kézdy, F. J., Heinrikson, R. L., Grimshaw, C. E., & Doughty, C. C. (1990) *J. Biol. Chem. 265*, 3628–3635.
Schowen, R. L. (1978) in *Transition States of Biochemical Processes* (Gandour, R. D., & Schowen, R. L., Eds.) pp 77–114, Plenum Press, New York.
Sorenson, P. E. (1972) *Acta Chem. Scand. 26*, 3357–3365.
Stinson, R. A., & Holbrook, J. J. (1973) *Biochem. J. 131*, 719–728.
Sugrobova, N. P., Kurganov, B. I., Gurevich, V. M., & Yakolev, V. A. (1972) *Mol. Biol. (Engl. Transl.) 6*, 217–231.
Sugrobova, N. P., Kurganov, B. I., & Yakolev, V. A. (1974) *Mol. Biol. (Engl. Transl.) 8*, 569–574.
Torreilles, J., Guêrin, M.-C., Dussossoy, D., & Crates de Paulet, A. (1983) *Biochimie 65*, 295–298.
Turner, A. J., & Flynn, T. G. (1982) *Prog. Clin. Biol. Res. 114*, 401–402.
Velick, S. F. (1958) *J. Biol. Chem. 233*, 1455–1467.
Walton, D. J. (1973) *Biochemistry 12*, 3472–3478.
Wermuth, B., Munch, J. D. B., & von Wartburg, J.-P. (1977) *J. Biol. Chem. 252*, 3821–3828.